Design and analysis of aerostatic spindle with high load characteristics for large ultra-precision drum lathe

Dongxu Wu[1], Bo Wang[1,*], Xichun Luo[2], Zheng Qiao[1]

1. Center for Precision Engineering, Harbin Institute of Technology, Harbin, 15001, P. R. China

2. Centre for Precision Manufacturing, Department of Design, Manufacture and Engineering Management, Faculty of Engineering, University of Strathclyde, Glasgow G1 1XJ, UK.

Bo Wang, Center for Precision Engineering, Harbin Institute of Technology, 92 West Dazhi Street, Nan Gang District, Harbin, 15001, P. R. China. Email: bradywang@hit.edu.cn, telephone number: +86-0451-86415244

Abstract

Aerostatic spindles offer low heat generation and high rotation accuracy which make them an ideal choice for ultra-precision drum lathe where extremely high motional accuracy and thermal stability are required. However, the limitations such as insufficient load capacity and stiffness have restricted their permissible application range and make them not suitable for large ultra-precision machine tools including drum lathe. In order to improve the load capacity and stiffness, this paper presents a high load capacity aerostatic spindle with pocketed orifice-type restrictors. Fluent is adopted and three-dimensional simulation models of aerostatic spindle with orifice and feeding pocket are set up to analyse the load characteristics. The simulation results show that this restrictor can enhance the throttling effect of orifice and suppress the pressure drop away from the orifice. Moreover, for aerostatic journal bearing, when eccentricity ratio is in the range of 0.2-0.3 and gas supply pressure is 0.6 MPa, carrying capacity and stiffness can reach up to 9499.4 N and 2813.1 N/μm. Finally, a group of loading experiments are carried out which prove that the novel three-dimensional simulation method is feasible and accurate to calculate the load characteristics of aerostatic spindles.

Keywords

Ultra-precision, aerostatic spindle, orifice-type restrictor, carrying capacity, stiffness

1. Introduction

Ultra-precision machine tools have various applications in manufacturing some components with optical quality surfaces, microstructured surfaces or free-form surfaces [1-3]. Ultra-precision drum lathes play an important role in machining large-scale microstructured drum molds [4-6] which are widely used in roll-to-roll process for mass production of TFT panel films and antireflective polymer optical film etc. [7, 8]. These machine tools are required to possess high structural stiffness, load capacity and position accuracy, as well as good damping property and thermal stability in order to maintain long term machining accuracy. For example, microstructures of 20 μm must be generated on the drum molds over a length of 2000 mm with form accuracy of 5 μm, and the pitch variation should be less than ±0.2 μm for one particular application [9]. Currently, due to high productivity and cost reduction in manufacturing microstructured surfaces, the drum molds than 2000 mm long are increasingly required in the market. The weight of such drum molds can even reach 1000 kg which proposes extremely high requirements in carrying capacity and stiffness for the machine tool spindles. As a result, oil hydrostatic spindles are normally adopted in large ultra-precision drum lathes to achieve high carrying capacity up to 3000 kg and stiffness more than 850 N/μm [10]. However, thermal deformation of oil hydrostatic bearing will cause excessive pitch error on the machined microstructures and degrade machining accuracy [11]. Compared with oil hydrostatic bearings, aerostatic bearings have the advantages of small friction, low heat generation and high rotation accuracy, etc. Aerostatic bearing is named as externally pressurized gas bearing. When it is working at a low rotating speed, macroscopic property behaved by the aerostatic effect of the high pressurized gas will play a dominant role in load characteristics [12]. Even if aerostatic bearings have been widely used in ultra-precision machine tools and precision instruments for aviation and aerospace industries, some limitations such as insufficient load capacity and

stiffness have restricted their permissible application, especially in large ultra-precision drum lathe. This is because excessive gas supply pressure will result in a supersonic zone, which can lead to a sudden drop in carrying capacity. In addition, during the design of aerostatic bearing, choosing incompatible bearing parameters, such as diameter of orifice and gas film thickness, will cause self-excited vibration. In this case, bearing cannot work normally, especially for high pressure and heavy load gas bearings [13, 14]. Moreover, the pneumatic or whirl instability is likely to occur if aerostatic journal bearing is working at very low or high speed [15]. Therefore, how to improve the load capacity and stiffness is very important to the promotion and application of aerostatic bearings.

Yoshimoto [16] used the elastic deformation of O-ring to achieve higher static stiffness and greater load capacity. Compared with rigid support, the O-ring could present a lower viscous resistance below the rotor and a larger pressure reduction rate above the rotor in the axial direction. However, the structure and installation were more complicated than conventional point source bearings. Additionally, several previous investigations proved that porous resistance inserted in feeding system could improve the load characteristics, but gas flow characteristics of porous material had not been fully understood, and the design and fabrication of the porous material also added more complexity [17-19]. The research result of Du et al. [20], who studied the relationship between pressure-equalizing groove and load characteristics of aerostatic journal bearings, showed that pressure-equalizing groove both in circumferential and axial directions could improve the load capacity and stiffness. Long et al. [21] carried out some research on the entrance effect of aerostatic thrust bearing, and the research results showed that for orifice compensated aerostatic bearing, feeding pocket can improve load capacity with the same geometric parameters. However, appropriate bearing parameters have to be chosen correctly. Even though a great deal of excellent research works has been carried out in order to improve

carrying capacity and stiffness of the aerostatic bearing, it remains a big challenge in the design of large scale and heavy load aerostatic bearing, especially for aerostatic journal bearing. As mentioned above, oil hydrostatic spindles are normally adopted on large ultra-precision drum lathe due to the high load capacity and stiffness. However, the cooling devices must be installed in the oil hydrostatic spindles to decrease the thermal deformation. Development of new design and analysis approach for high carrying capacity and stiffness aerostatic bearings therefore, becomes an important task for large ultra-precision drum lathe.

For this aim, the flow characteristics of lubricating gas in restrictor should be analyzed in order to fully understand the load characteristics of aerostatic bearing. Fourka et al. [22] presented a non-linear model for the stability analysis of air thrust bearing. The model was based on the finite element method, and the calculated stability threshold by the non-linear model was more precise compared with the linear analysis. The experimental study conducted by Belforte et al. [23] showed that for different types of orifice, such as annular orifice and simple orifice with feeding pocket, the flow characteristics could be described by using different discharge coefficients. Neves et al. [24] believed that the value of the orifice discharge coefficient was variable as a function of the pressure ratio, orifice throat discharge and supply pressures since feeding orifices could operate at either sonic or subsonic flow conditions. Yang et al. [15] studied the stability threshold and critical whirl ratio of a rigid rotor-aerostatic bearing system using the perturbation method and eigen-solution method. Dong et al. [25] adopted differential quadrature method to discretize the Reynolds equation as a series of algebraic equations, which could be used to analyze the load performance of aerostatic thrust bearings.

The manufacturing errors have a significant effect on the air flow and bearing performance of aerostatic bearings. Pande and Somasundaram [26] reported that the deviations in bearing surfaces from the ideal geometry significantly affected the performance

characteristics of aerostatic journal bearings. As a result, form errors reduced the load capacity by 10-12%, and surface roughness decreased the load capacity by 15-20% and decreased the flow rate by 10-12% compared with a smooth bearing. Khalil and El-Shorbagy [27] pointed out that surface roughness reduced the lubricant flow rate and increased the frictional power. Kwan and Post [28] believed that both static load and stiffness are sensitive to the manufacturing error such as surface form errors and changes in orifice diameter.

As the computational fluid dynamics (CFD) software is emerging, the analytical approach of aerostatic bearings' performance has become more diverse. Renn et al. [29] proposed a new model of the mass flow rate characteristic through an orifice in the aerostatic bearing through experimental and CFD simulation study. Compared with the conventional model, the value of the critical pressure ratio was the major difference. Li et al. [30] conducted a simulation and experimental research which showed that aerostatic thrust bearing would have good performance if orifice diameter and film thickness were small, while air chamber diameter was big. Although many efforts have been made to study the load performance of aerostatic bearings, there are still some areas that need improvement. Few literatures have conducted the three-dimensional models and analysis of aerostatic spindle. The two-dimensional simulation method of CFD study is mainly focused on aerostatic thrust bearing [29, 30], while little attention has been paid to aerostatic journal bearing. Moreover, conventional numerical approaches have ignored the flow process of lubricating gas in orifice and feeding pocket, which also has a significant effect on load characteristics of aerostatic bearing. Hence, the methods mentioned cannot accurately perform the gas flow characteristics in aerostatic bearings.

This paper presents an orifice-type aerostatic spindle of which the restrictor is specially designed with orifice and feeding pocket. In order to fully take account of the influence of flow properties of the lubricating gas on load characteristics, this paper has

adopted computational fluid dynamics (CFD) software, Fluent as a new analysis tool. Three-dimensional simulation models of aerostatic journal bearing and aerostatic thrust bearing are set up in this paper. Furthermore, the gas pressure distributions in orifice, feeding pocket and gas film are presented and the load characteristics of the aerostatic spindle are fully analyzed. Finally, in order to validate the simulation results, some loading experiments on load performance of the aerostatic spindle are carried out.

2. Design and manufacturing of aerostatic spindle

2.1 Structural design of aerostatic spindle

In this paper, a new aerostatic spindle with orifice-type restrictors is designed in order to achieve both high carrying capacity and high stiffness. Figure 1(a) shows the internal structure of the aerostatic spindle and Figure 1(b) is the photograph of the spindle sleeve. This spindle consists of aerostatic journal bearing and close-type aerostatic thrust bearing. Aerostatic journal bearing has four-row orifice-type restrictors, and there are 12 orifices in each row. Aerostatic thrust bearing adopts close-type circular structure, and it has two thrust surfaces, one is machined on the end surface of the aerostatic journal bearing, and the other one is on the end surface of the thrust plate. This kind of aerostatic thrust bearing can have bidirectional carrying capacity in axial direction. In order to improve carrying capacity and stiffness, the orifice-type restrictor is specially designed with orifice and feeding pocket. Figure 1(c) shows the structure diagram of orifice-type restrictor. The restrictor is inset in the hole of spindle sleeve. The depth of feeding pocket h_2 is precisely controlled through restrictor's mounting position. Table 1 gives the structural parameters of the aerostatic journal bearing and the aerostatic thrust bearing.

2.2 Manufacturing of aerostatic bearings

Manufacturing errors such as form errors and surface roughness can affect the air flow and can reduce the bearing performance and lifespan of aerostatic bearings [26-28]. The

material of aerostatic bearings is 38CrMoAl. To achieve the good manufacturing quality, the various machining processes are adopted. First, the workblank of aerostatic bearing is processed by rough turning and finish turning. Then, the bearing rotor and thrust surfaces are grinded in precision grinding machine. Sequently the bearings are treated with quenching and nitriding technique to harden the surfaces. Finally, through lapping and polishing by hand, the surface roughness Ra is less than 500 nm.

3 Method

In this paper, three-dimensional models of aerostatic journal bearing and aerostatic thrust bearing are set up by using Computational Fluid Dynamics (CFD) software, Fluent. Both macroscopic and microscopic properties of the gas flow field are presented for pressure distribution in different locations of the bearing clearance.

3.1 Simulation models for aerostatic spindle

The aerostatic spindle used in large ultra-precision drum lathe comprises aerostatic journal bearing and aerostatic thrust bearing. The simulation models represent gas flow field in orifice, feeding pocket and gas film. Because aerostatic journal bearing are symmetrical in the axial direction, half model of aerostatic journal bearing is built to simplify the modelling and calculation process. Aerostatic thrust bearing is symmetrical along the circumferential direction, so 1/12 model of the aerostatic thrust bearing is enough to present the load characteristics of the whole bearing. Compared with the two-dimensional Cartesian coordinate models [29, 30], the three-dimensional simulation models are more complex to establish. Figure 2 shows the mesh model of the aerostatic journal bearing. Due to non-uniform thickness of the cylindrical gas film in aerostatic journal bearing's clearance, it is very difficult to achieve high-quality mesh model which, however, has a significant influence on the calculation accuracy. For example, the skewness of mesh elements is an important factor which can evaluate the mesh quality. The mesh elements with high skewness not only

cause computational divergence, but also result in big residuals. For the simulation models of aerostatic bearings, if the skewness of mesh elements is in the range of 0.8-0.9, the residuals will be in the range of 10^{-1}-10^{-2} even when the solution converges. In order to solve this problem, the whole bearing models have been split into small pieces, and then each piece are meshed separately. Hence, this half model consists of many split parts, and hexahedral mesh is chosen for all the models, as well as the same treatment used for the aerostatic thrust journal as shown in Figure 3. Because the gas pressure gradient in orifice and feeding pocket can change significantly and the flow field in restrictor is more complex, here the meshes are refined as shown in Figure 4. In this paper, the skewness of all mesh elements of aerostatic bearings is less than 0.68. As a result, the maximum residuals for each of the conserved variables are less than 10^{-4}.

3.2 Boundary conditions and parameters

For boundary conditions, the inlet face in restrictor is treated as pressure-inlet, outlet face is treated as pressure-outlet, the symmetrical part is set up to symmetry, and all the other outside surfaces are wall by default [30]. After the bearing models and boundary conditions are finished, the simulation parameters will be set for calculation. Spalart-Allmaras model is chosen as viscous model, and the pressure-velocity coupling algorithm adopts SIMPLE in solution controls. During the calculation process, monitoring of the scaled residuals and the mass flow rate of the inlet and outlet face is necessary to judge whether the result is convergent and acceptable.

4 Results and analysis

In this research, the three-dimensional pressure distribution of lubricating gas is fully analyzed. Compared with the two-dimensional simulation models [29, 30], the three-dimensional simulation models are more capable of reflecting the true characters of the gas

flow field in each position of bearing clearance. This is especially important when analyzing the load characteristics of the aerostatic journal bearing.

4.1 Pressure distribution of lubricating gas

Figure 5 shows the gas film pressure contour of the aerostatic journal bearing, and the pressure of the lower part is obviously larger than that of the upper part. The reason is that the gas film thickness of the lower part in bearing clearance is smaller than that of the upper part, and the smaller gas film thickness has the larger pressure distribution. The orifice area has the largest pressure distribution, and the area between these tow-row orifices has stable and large-area load region. Closer to outlet boundary, gas film pressure gradually decreases to the atmospheric pressure. Figure 6 show the gas film pressure contour of the aerostatic thrust bearing. When there is an axial load on the bearing rotor, the offset of thrust plate will result in different gas film thickness on the two thrust surface, so it is the different pressure of gas film that enables close-type aerostatic journal bearing to have the load capacity. The orifice-type restrictor consists of the orifice and the feeding pocket. The feeding pocket can enhance the throttling effect of the orifice, and suppress the pressure drop away from the orifice. Figure 7 shows the gas pressure contour in the cross-sectional area of the orifice-type restrictors without feeding pocket and with feeding pocket. If the restrictor does not have a feeding pocket, the gas pressure will decrease from the border of the orifice and gas film, and gradually go down to the atmospheric pressure. However, if the restrictor has a feed pocket, the gas pressure will decrease from the border of the feeding pocket and gas film. In the feeding pocket, there is a stable high-pressure zone, and this high-pressure zone can improve the carrying capacity and stiffness of the aerostatic bearings.

4.2 Load characteristics of aerostatic journal bearing

This section discusses the influence of gas supply pressure and eccentricity ratio on the carrying capacity and stiffness. According to the actual operating conditions, the gas supply

pressure is adjusted within the range of 0.4 MPa-0.6 MPa, and the eccentricity ratio is determined by the external load, which is in the range of 0-0.4. Figure 8 shows the load characteristics of the aerostatic journal bearing. It can be seen that, as eccentricity ratio increases, carrying capacity will gradually increase, and almost present linear growth when eccentricity ratio is 0-0.2. However, stiffness decreases with the increase of the eccentricity ratio. This trend is particularly evident when eccentricity ratio is more than 0.2. The similar result can be found in some literature [20]. Additionally, carrying capacity and stiffness will both increase with the increase of the gas supply pressure, but excessive gas supply pressure will cause supersonic zone. Considering both carrying capacity and stiffness, it is reasonable that the eccentricity ratio is in the range of 0.2-0.3 and the gas supply pressure is 0.6 MPa. In this case, the carrying capacity and stiffness can reach up to 9499.4 N and 2813.1 N/μm, respectively. Since there are two aerostatic spindles separately in headstock and tailstock, the drum lathe proposed in this paper has the ability of bearing the drum workpiece up to 1000 kg weight.

4.3 Load characteristics of aerostatic thrust bearing

As shown in Figure 9, some load characteristics of the aerostatic thrust bearing can be drawn. First, due to the close-type structure, there is no carrying capacity if the thrust plate does not have any deflection in the axial direction. With the offset of the thrust plate and gas supply pressure increases, carrying capacity will increase significantly. Second, stiffness has also grown along with the rising of the gas supply pressure, while it presents a downward trend as the offset of the thrust plate rises. This downward trending is more obvious when the offset of the thrust plate is in the range of 2-4 μm and 5-6 μm. Because this ultra-precision drum lathe has a horizontal layout structure, the axial load is much smaller than the radial load. When the offset of the thrust plate is 3 μm and the gas supply pressure is 0.6 MPa,

carrying capacity and stiffness is 7149.6 N and 2154 N/μm, which can meet the requirements of large ultra-precision drum lathe.

5 Experimental Verification

5.1 Experimental setup

In order to validate the simulation results, some loading experiments of the aerostatic spindle are carried out. The rotor system of this drum lathe consists of motor rotor, spindle rotor, connection, chuck and drum workpiece. Due to the horizontal structure, the radial load performance of the lathe becomes very important. Therefore, the load characteristics of the aerostatic journal bearing are measured in the loading experiments. Considering the difficulty of generating such a heavy load, installing different weight drum workpieces is adopted to realize the different loads, and three groups of experiments are carried out. The experimental setup is shown in the Figure 10. For the first group of experiments as shown in Figure 10(a), there is no drum workpiece installed on the drum lathe. In this case, the load performance of only headstock spindle is measured. The load includes motor rotor, spindle rotor, connection, chuck, the weight of which is 186 kg. For the other two groups of experiments, the 140 kg and 300 kg drum workpiece are respectively installed on the drum lathe as shown in Figure 10(b) and Figure 10(c), and in these two cases the headstock spindle and tailstock spindle provide the carrying capacity. Hence, the loads of 1860 N, 2560 N, 3360 N for one spindle are generated by the workpieces of different weights. The vertical displacements of the chuck and the drum workpiece are respectively measured by a laser displacement sensor (Micro-Epsilon optoNCDT2220LL), which has a measuring range of 2 mm and a resolution of 30 nm.

5.2 Analysis of experimental results

In the loading experiments, the eccentricity ratio of rotor is the measured values at a fixed load by adjusting the gas supply pressure to 0.35 MPa, 0.40 MPa, 0.45MPa, and 0.50 MPa, and each data is measured repeatedly six times. The simulation and experimental

results are shown in Figure 11, where the lines depict the simulation values, and the discrete points depict the experimental values. In general, the simulation results are in good agreement with the experimental results. The maximum standard deviation is 0.011, and the ratio of the maximum standard deviation to the corresponding mean value of eccentricity ratio is within 6.6%. The maximum deviation of the simulation values and experimental values is less than 15.3%. Therefore, the efficiency and accuracy of the simulation method for calculating the load characteristics of aerostatic bearings has been experimentally proved.

6 Conclusions

This paper presents the design and analysis of an orifice-type aerostatic spindle with high carrying capacity and stiffness used for a large ultra-precision drum lathe. The novel three-dimensional simulation models of aerostatic journal bearing and aerostatic thrust bearing are developed using Fluent, and the load characteristics of the aerostatic spindle are studied. Finally, the experimental verification is carried out which proves that this simulation method is feasible and can accurately calculate the load characteristics of the aerostatic bearings. Based on the results of simulation and experimental studies, the conclusions can be drawn as follows:

(1) The proposed three-dimensional simulation models can accurately reflect the gas flow characteristics in bearing clearance.

(2) If the restrictor has a feeding pocket, the gas pressure will decrease from the border of the feeding pocket and gas film. In feeding pocket, there is a stable high-pressure area, which can suppress the pressure drop away from the orifice. Hence, the improved throttling effect of orifice can enhance the load capacity and stiffness.

(3) For aerostatic journal bearing, it is reasonable that eccentricity ratio is in the range of 0.2-0.3 and gas supply pressure is 0.6 MPa. In this case, carrying capacity and stiffness can reach up to 9499.4 N and 2813.1 N/μm, which can meet the requirements of large ultra-

precision drum lathe.

Acknowledgement

The authors gratefully acknowledge the financial support of National Science and Technology Major Project of High-end CNC Machine Tools and Basic Manufacturing Equipment of China and the Aviation Science Foundation Project. The first author also would like to thanks the EPSRC (EP/K018345/1) and University of Strathclyde to provide sponsorship for the visiting research in the UK.

Funding

The research is supported by National Science and Technology Major Project of High-end CNC Machine Tools and Basic Manufacturing Equipment of China (grant number 2011ZX04004-021); and the Aviation Science Foundation Project (grant number 20110877007).

References

1. Weck M, Fischer S and Vos M. Fabrication of microcomponents using ultraprecision machine tools. *Nanotechnol* 1997; 8: 145-148.
2. Luo XC, Cheng K, Webb D, et al. Design of ultraprecision machine tools with applications to manufacture of miniature and micro components. *J Mater Process Technol* 2005; 167: 515-528.
3. Park CH, Song CK, Hwang J, et al. Development of an ultra precision machine tool for micromachining on large surfaces. *Int J Precis Eng Manuf* 2009; 10: 85-91.
4. Lee JC, Gao W, Shimizu Y, et al. Precision measurement of carriage slide motion error of a drum roll lathe. *Precis Eng* 2012; 36: 244-251.
5. Lee JC, Gao W, Shimizu Y, et al. Spindle error motion measurement of a large precision roll lathe. *Int J Precis Eng Manuf* 2012; 13: 861-867.

6. Lee JC, Shimizu Y, Gao W, et al. Precision evaluation of surface form error of a large-scale roll workpiece on a drum roll lathe. *Precis Eng* 2014; 38:839-848.
7. Wang MW, Tseng CC. Analysis and fabrication of a prism film with roll-to-roll fabrication process. *Opt Express* 2009; 17: 4718-4725.
8. Ting CJ, Chang FY, Chen CF, et al. Fabrication of an antireflective polymer optical film with subwavelength structures using a roll-to-roll micro-replication process. *J Micromech Microeng* 2008; 18: 1-9.
9. Oh JS, Song CK, Hwang J, et al. An Ultra-precision Lathe for Large-area Micro-structured Roll Molds. *J Korean Soc Precis Eng* 2013; 30: 1303-1312.
10. Moore Nanotechnology Systems. http://www.nanotechsys.com/machines/nanotech-hdl-2000-horizontal-drum-lathe/.
11. Je TJ, Jeon EC, Park SC, et al. Improvement of machining quality of copper-plated roll mold by controlling temperature variation. *Trans Nonferrous Met Soc China* 2011; 21: 37-41.
12. Liu ZS, Zhang GH, and Xu HJ. Performance analysis of rotating externally pressurized air bearings. *Proc IMechE Part J: J Engineering Tribology* 2009; 223: 653-663.
13. Du JJ, Liu D, Zhang GQ, et al. Study of self-excited vibration for externally pressurized gas thrust bearing with circumferential groove. *Lubr Eng* 2010; 35: 9-12.
14. Ye YX, Chen XD, Hu YT, et al. Effects of recess shapes on pneumatic hammering in aerostatic bearings. *Proc IMechE Part J: J Engineering Tribology* 2010; 224: 231-237.
15. Yang DW, Chen CH, Kang Y, et al. Influence of orifices on stability of rotor-aerostatic bearing system. *Tribol Int* 2009; 42: 1206-1219.
16. Yoshimoto S. Improvement of static characteristics of an aerostatic journal bearing using the elastic deformation of an O-ring. *Tribol Int* 1987; 20: 290-296.

17. Fourka M and Bonis M. Comparison between externally pressurized gas thrust bearings with different orifice and porous feeding systems. *Wear* 1997; 210: 311-317.
18. Yoshimoto S, Tozuka H and Dambara S. Static characteristics of aerostatic porous journal bearings with a surface-restricted layer. *Proc IMechE Part J: J Engineering Tribology* 2003; 217: 125-132.
19. Panzera TH, Rubio JC, Bowen CR, et al. Microstructural design of materials for aerostatic bearings. *Cem Concr Compos* 2008; 30: 649-660.
20. Du JJ, Zhang GQ, Liu T, et al. Improvement on load performance of externally pressurized gas journal bearings by opening pressure-equalizing grooves. *Tribol Int* 2014; 73: 156-166.
21. Long W and Bao G. Entrance effect on load capacity of orifice compensated aerostatic bearing with feeding pocket. *Chin J Mech Eng* 2010; 23: 1-9.
22. Fourka M, Tian Y and Bonis M. Prediction of the stability of air thrust bearings by numerical, analytical and experimental methods. *Wear* 1996; 198: 1-6.
23. Belforte G, Raparelli T, Viktorov V, et al. Discharge coefficients of orifice-type restrictor for aerostatic bearings. *Tribol Int* 2007; 40: 512-521.
24. Neves MT, Schwarz VA and Menon GJ. Discharge coefficient influence on the performance of aerostatic journal bearings. *Tribol Int* 2010; 43: 746-751.
25. Dong ZG, Ding Y, Liu PK, et al. On the analysis of aerostatic thrust bearings with the differential quadrature method. *Proc IMechE Part J: J Engineering Tribology* 2014; 228: 232-240.
26. Pande SS and Somasundaram S. Effect of manufacturing errors on the performance of aerostatic journal bearings. *Wear* 1981; 66: 145-156.
27. Khalil MF and El-Shorbagy KA. Surface roughness effects on externally pressurized bearing performance. *Wear* 1985; 103: 1-10.

28. Kwan YBP and Post JB. A tolerancing procedure for inherently compensated, rectangular aerostatic thrust bearings. *Tribol Int* 2000; 33: 581-585.
29. Renn JC and Hsiao CH. Experimental and CFD study on the mass flow-rate characteristic of gas through orifice-type restrictor in aerostatic bearings. *Tribol Int* 2004; 37: 309-315.
30. Li YT and Ding H. Influences of the geometrical parameters of aerostatic thrust bearing with pocketed orifice-type restrictor on its performance. *Tribol Int* 2007; 40: 1120-1126.

Figure captions

Figure 1. Aerostatic spindle with orifice-type restrictors: (a) Internal structure of aerostatic spindle; (b) Spindle sleeve; (c) Orifice-type restrictor with feeding pocket with D_1 = 6 mm, D_2 = 4 mm, d=0.2 mm, h_1= 0.5 mm, h_2=0.2 mm.

Figure 2. Mesh model of aerostatic journal bearing.

Figure 3. Mesh model of aerostatic thrust bearing.

Figure 4. Refined meshes in orifice and feeding pocket.

Figure 5. Gas film pressure contour of aerostatic journal bearing, when gas supply pressure is 0.5 MPa, the eccentricity ratio is 0.3.

Figure 6. Gas film pressure contour of aerostatic thrust bearing, when gas supply pressure is 0.5 MPa, the offset of thrust plate is 3 μm.

Figure 7. Gas pressure contour of orifice-type restrictor: (a) Orifice-type restrictor without feeding pocket; (b) Orifice-type restrictor with feeding pocket.

Figure 8. Load characteristics of aerostatic journal bearing: (a) Carrying capacity; (b) Stiffness.

Figure 9. Load characteristics of aerostatic thrust bearing: (a) Carrying capacity; (b) Stiffness.

Figure 10. Experimental setup: (a) No drum workpiece installed on the lather; (b) A drum workpiece of 140 kg installed on the lathe; (c) A drum workpiece of 300 kg installed on the lathe.

Figure 11. Comparison of simulation values and experimental values: (a) Gas supply pressure is 0.35 MPa; (b) Gas supply pressure is 0.40 MPa; (c) Gas supply pressure is 0.45MPa; (d) Gas supply pressure is 0.5 MPa.

Table options

Table 1. Structural parameters of the aerostatic spindle.

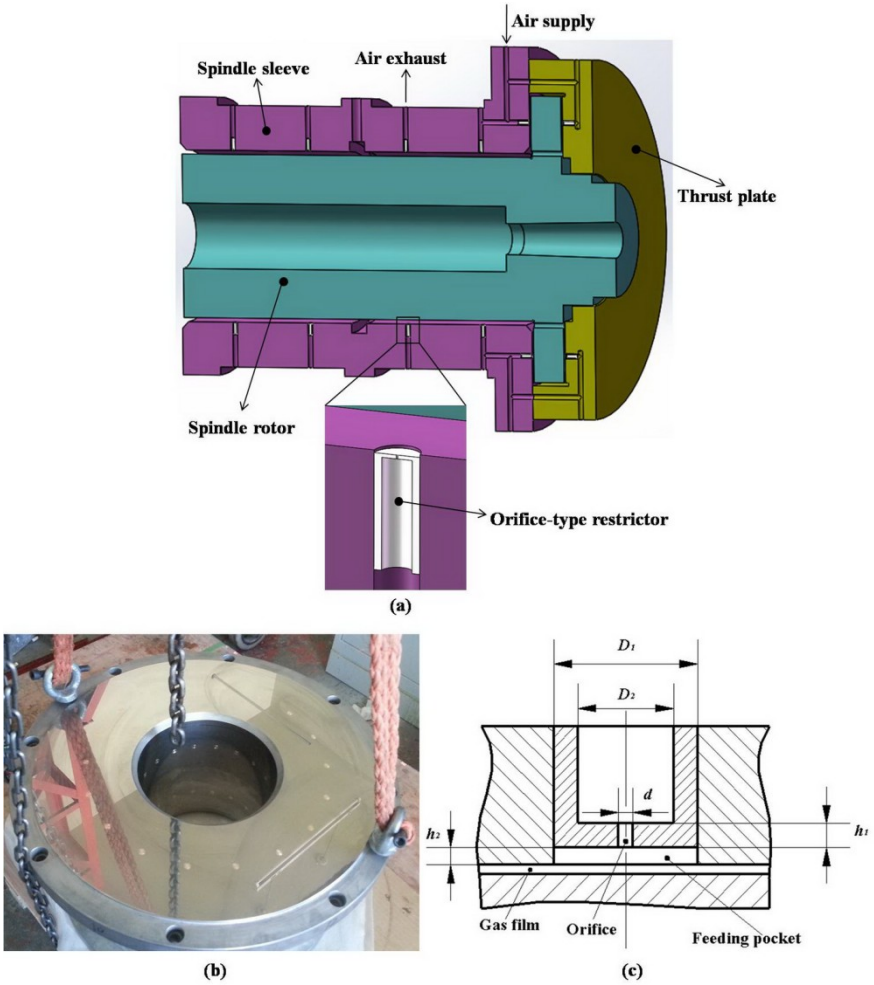

Figure 1.Aerostatic spindle with orifice-type restrictors: (a) Internal structure of aerostatic spindle; (b) Spindle sleeve; (c) Orifice-type restrictor with feeding pocket with D_1 = 6 mm, D_2 = 4 mm, d=0.2 mm, h_1= 0.5 mm, h_2=0.2 mm.

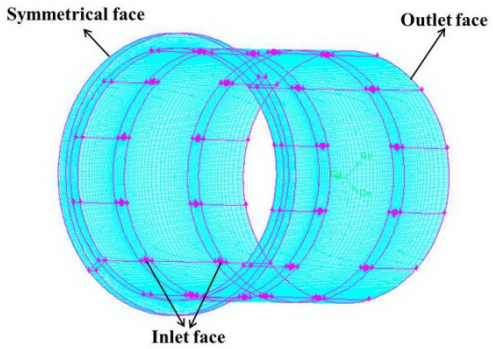

Figure 2

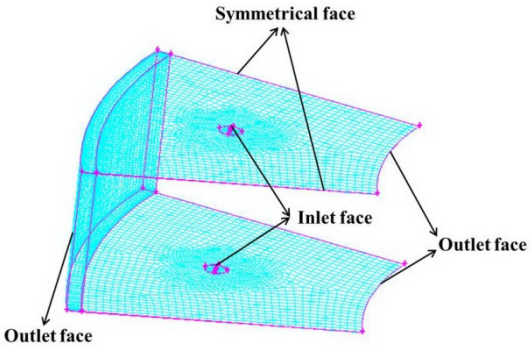

Figure 3

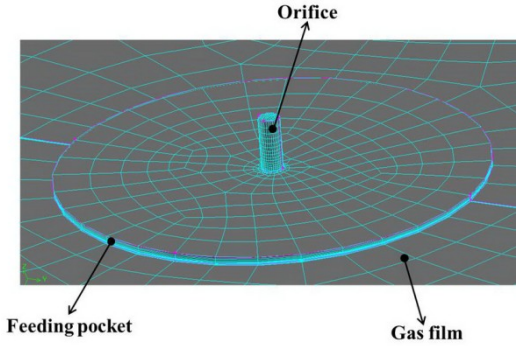

Figure 4

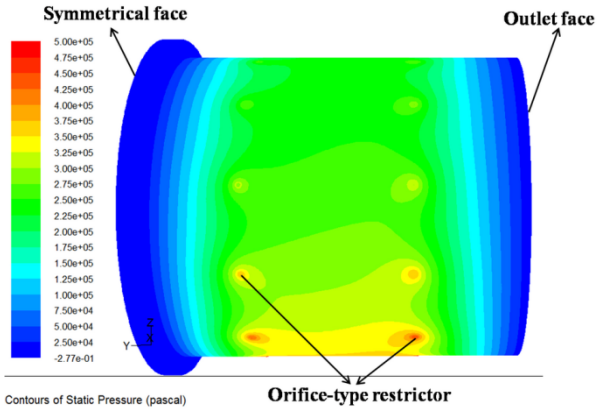

Figure 5

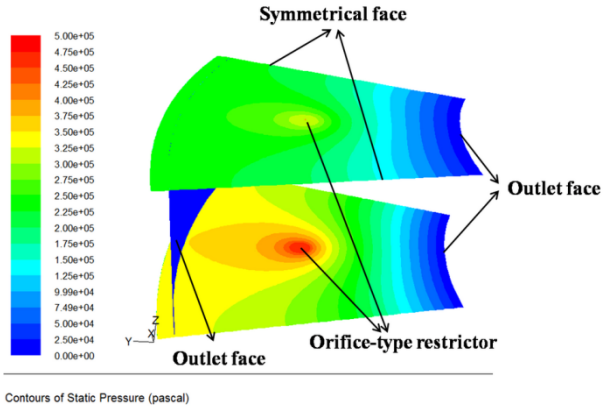

Figure 6

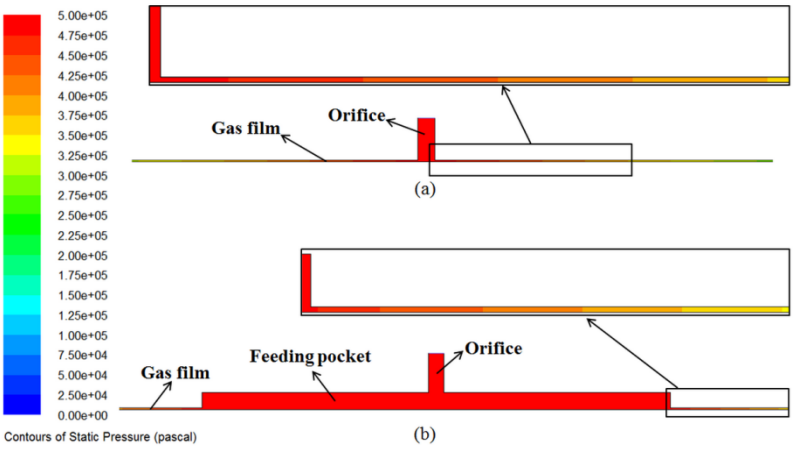

Figure 7

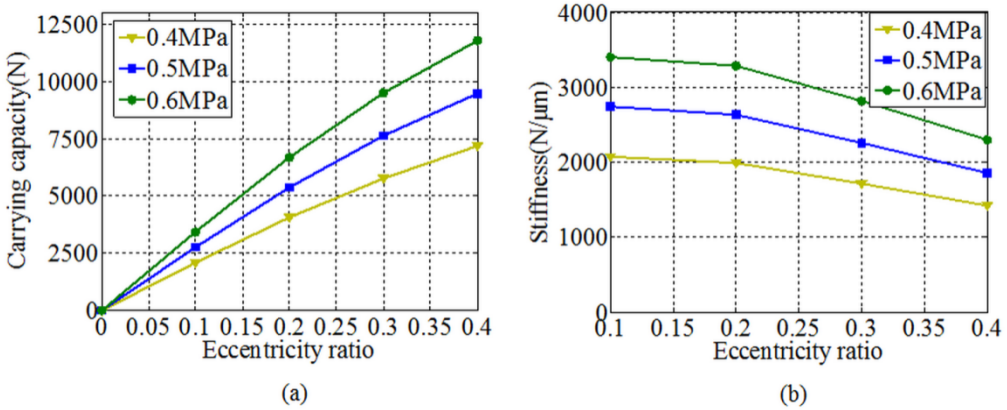

Figure 8

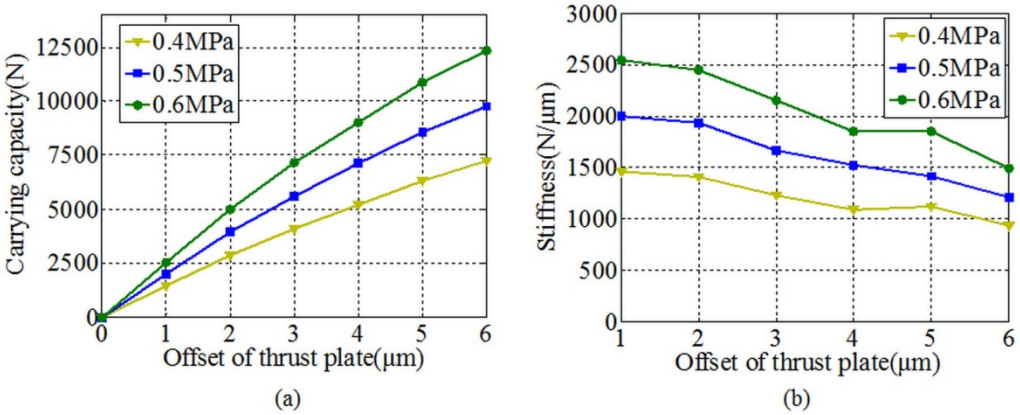

Figure 9

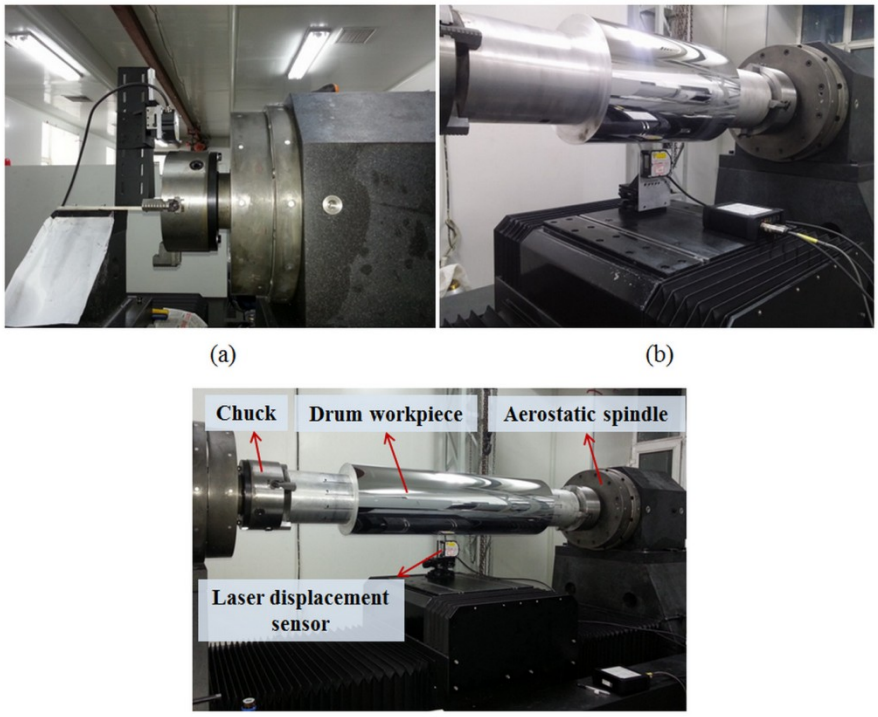

Figure 10

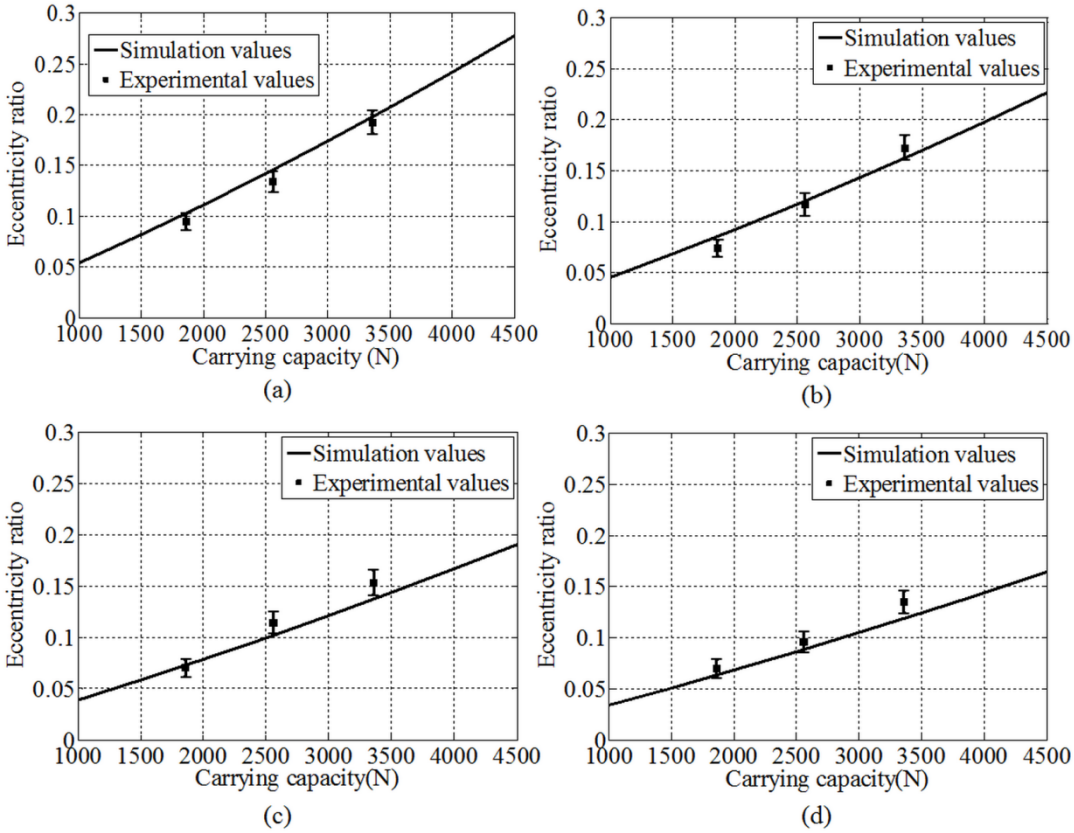

Figure 11